Velocity Effect Sensitivity Analysis of Ball-end Milling Ti-6Al-4V

Anshan Zhang (aszhang@hrbust.edu.cn)
Harbin University of Science and Technology https://orcid.org/0000-0002-4070-0701
Xianli Liu
Harbin University of Science and Technology
Caixu Yue
Harbin University of Science and Technology
Rongyi Li
Harbin University of Science and Technology
Steven Y. Liang
Georgia Institute of Technology
Lihui Wang
KTH Royal Institute of Technology

Research Article

Keywords: Ball-end milling, Velocity effect, Ploughing, Feed direction selection

Posted Date: July 8th, 2021

DOI: https://doi.org/10.21203/rs.3.rs-681959/v1

Velocity Effect Sensitivity Analysis of Ball-end Milling Ti-6Al-4V*

Anshan Zhang [1*], Xianli Liu [1], Caixu Yue [1], Rongyi Li [1], Steven Y. Liang [2], Lihui Wang [3]

(1 Key Laboratory of Advanced Manufacturing and Intelligent Technology, Ministry of Education, Harbin University of Science &Technology, Harbin 150080, People's Republic of China

2 George W. Woodruff School of Mechanical Engineering, Georgia Institute of Technology, Atlanta 30332, USA

3 KTH Royal Institute of Technology, Stockholm 25175, Sweden)

Abstract: Ball-end cutters are widely used in industries of dies, molds, and aerospace, which have the problem of poor machined surface quality due to the low cutting speed near the tool-tip. With the increase in the complexity of parts, it will become more and more difficult to avoid the tool-tip participating in the cutting. In this paper, the velocity effect sensitivity of ball-end cutter is analyzed, and several key positions, including the intersection points of the CWE boundaries, are selected to describe the cutting speed in three dimensions. The relationships between the cutting speed of the critical points and important variables such as: machining inclination angle and the feed direction were investigated. The optimal range of feed direction is obtained when the tool-tip engages in the contact circle. The core aim of the feed direction selection is to make the tool engagement area in a high position by changing the feed direction, to avoid surface damage caused by ploughing and improve the quality of the machined surface. Finally, an experimental study was carried out, and the results corroborate the effectiveness of the selection method. In the experiment, it was also found that cutting-out from the cutter contact position can improve the surface quality in the directions of non-optimal range, and the milling force and chips shape will vary with the change of the feed direction.

Keywords: Ball-end milling; Velocity effect; Ploughing; Feed direction selection;

Declarations

Funding

This research was funded by Projects of the International Cooperation and Exchanges for National Science Foundation of China (Grant Number 51720105009) and the National Key Research and Development Project of China (Grant Number 2019YFB1704800).

We have no conflict of interest to declare.

Conflicts of interest/Competing interests

The authors declare that there is no conflict of interests regarding the publication of this article.

Availability of data and material

The datasets used or analyzed during the current study are available from the corresponding author on reasonable request.

Code availability (Not applicable)

Authors' contributions

Anshan zhang: Conceptualization, Methodology, Software, Writing- Original draft preparation; Xian-Li liu: Funding acquisition, Project administration, Writing - Review & Editing; Cai-Xu Yue: Data curation, Resources, Writing - Review & Editing; Rong-Yi Li: Data curation, Investigation, Visualization; Steven Y. Liang: Writing - Review & Editing; Lihui Wang: Writing - Review & Editing.

Ethics approval

The content studied in this article belongs to the field of metal processing, does not involve humans and animals. This article strictly follows the accepted principles of ethical and professional conduct.

Consent to participate

My co-authors and I would like to opt in to In Review.

* Corresponding author: Anshan Zhang

E-mail: aszhang@hrbust.edu.cn

Consent for publication

I agree with the Copyright Transfer Statement.

1 Introduction

Ball-end cutters are the most commonly used tools in finishing and semi-finishing operations of sculptured surfaces because they have the advantage of strong adaptability to the variation of surface curvature [1]. However, unlike the ordinary face milling machining, the cutter workpiece engagement (CWE) alternates constantly, which makes the process unstable. Due to the geometrical characteristics of this process, the effective cutting speed varies with the machining inclination angle (angle formed between cutter axis and surface normal direction) and feed direction [2]. Moreover, because the cutting speed at the tip of the tool is zero, the engagement of tool-tip into the cutting region is detrimental to the machining process, which causes the phenomenon of ploughing and the deterioration of surface quality [3]. Although the tool-tip engagement can be relatively avoided by adjusting the tool orientation in a 5-axis machining, when the cutter needs to be replaced, the part near the tool-tip which has not been involved in the cutting would still be new, thus resulting in a significant waste of the cutter material [4]. With the increase in the complexity of parts, it will become more and more difficult to avoid the tool-tip participating in the cutting. Therefore, when the tool-tip engages in the contact circle, the cutting mechanism and the chain reactions caused by the velocity effect of ball-end cutters need to be further studied to maximize the benefits of ball-end cutters.

The change of cutting speed will influence the final material characteristics and the chip forming mechanism [5,6], thus affecting the final surface quality, which is called “velocity effect” in related literature [7-9]. The speed effect was proposed by ROWE [7] in the field of grinding, which studied the influence of the ratio of the cutting speed of the grinding wheel to the feed rate of a workpiece in the process. Tian [8] mentioned the concept of velocity effect to explore the influence of increasing the linear speed of the grinding wheel on the chip forming process of high strength and tough materials. Liu [9] studied the influence of velocity effect on the minimum cutting thickness in the process of milling hardened steel with ball-end cutters and determined the minimum cutting thickness under different cutting speeds.

The parameters of cutter postures and tool path orientations will affect the tool engagement area, and different parts of the tool participating in cutting would lead to variations of cutting speed, hence affecting the surface quality. Lee et al. [10] performed the experiments at a workpiece tilt angle of 45° using various cutter orientations and materials, and the results indicated that the best cutting strategy was a vertical upward cutter orientation. Daymi et al. [11] did several experiments with ball-end milling in a titanium allow Ti-6Al-4V, they studied the effects of different workpiece tilt angle, feed per tooth, radial cutting depth, cutting speed, and other parameters on the surface topography. The experimental results show that better surface quality can be obtained when the inclination angle of the workpiece is 25°.

Kalvoda et al. [12] used 5-axis milling experiments to study the effects of tool posture on milling surface roughness and texture, residual stress, and surface microhardness. The results show that the tilt angle has a great influence on the surface roughness and residual stress, while the influence of the lead angle is relatively small. Yao et al. [13] studied the effects of cutting speed, feed per tooth, and radial cutting depth on the surface roughness of flank milling titanium alloy TB2 by orthogonal experiments, obtaining an empirical correlation between milling parameters and surface roughness. It is considered that the feed per tooth has the greatest influence on the surface roughness.

Shen et al [14] studied the influence of cutter path orientations on milling force, temperature, and surface integrity through the 60° incline surface milling tests of TC17. The results indicate that the maximum milling force is obtained under vertical downward milling path, and the minimum surface roughness is achieved under vertical upward mode, however, only the cutting speed at the tool contact point is considered in different tool paths.

Nicola et al. [15] carried out an experiment of milling H13 steel with ball-end cutters. They studied the influence of four different tool paths on the machined surface roughness and texture for an inclination angle of 60°.

It was concluded that the surface roughness is the largest when using vertical upward milling, and the smallest when using the vertical downward milling.

Aspinwall et al [16] carried out cutting experiments with 45° angle with the oblique plane and 0° angle with the horizontal plane. They measured the force, vibration, tool wear, and surface integrity in the cutting process. The experimental results show that the resultant cutting force is highest with the 0° workpiece tilt angle operation as a consequence of the ploughing action occurring at the center of the ball-end cutter. However, only the consistency of the highest cutting speed point was considered in the experiment, and the influence of the lowest cutting speed point in the engagement area on the machined surface was not considered.

Tan et al. [17] investigated the influence of tool feed direction on cutting force, tool wear, and surface integrity. They did the milling experiment with a 30° angle with the oblique plane for ball-end milling TC17. The experimental results show that the vertical upward tool path has the best surface morphology. Toh [18, 19] used a ball-end cutter to process the AISIH13 with a machined inclination angle of 75°. It deduced vertical downward orientation provided the long tool life, and vertical upward orientation achieved the best workpiece surface texture. Chen [20] carried out a series of experiments based on the analysis of cutting effect and response surface methodology. They analyzed various tool postures by geometric modeling and numerical simulation, however, the model did not consider the tool-tip effect in cutting.

In summary, the variables that affect the surface quality of ball-end cutters generally consider three general aspects: machining inclination (3-axis) or tool orientation (5-axis), tool path direction, and milling parameters (spindle speed, feed per tooth, cutting depth, etc.). The influence of the cutting speed of cutter contact point or maximum cutting speed have been mostly considered in previous researches, and the effects of various factors on the cutting process and machined surface have been previously studied. However, the conclusions obtained under different experimental conditions are different. When the tool attitude and path parameters vary, the actual cutter engagement area changes, and thus, the minimum cutting speed also changes. In the case of the tool-tip participating in cutting, the change of the minimum cutting speed will have a great impact on the quality of the machined surface [21]. Therefore, it is unreasonable to consider only the variation of a single point's cutting speed in the engagement area. Moreover, the case of cutting into and out within per tooth feed cycle has not been taken into account in previous researches, which also has a significant influence on the cutting process.

In this paper, several key points are selected to describe the change of cutting speed in the entire engagement area. A method for solving parameters of tool path direction is proposed, which is within the constraint condition of the cutter contact point i.e. the lowest cutting speed position in the engagement area. At the same time, the cutting into and out of the tool is considered to optimize the tool feed direction and improve the machining surface quality.

2 Sensitivity analysis of velocity effect in Cutter Workpiece Engagement

2.1 Cutter Workpiece Engagement (CWE) in ball-end milling

The purpose of introducing the CWE model in this part is to determine the actual cutting position of the tool, so that the cutting speed in the engagement area can be obtained under different tool postures. At present, many researches on CWE model have been carried out, mainly including the solid modeler method [22,23], the Z-map method [24,25] and the analytical method [26]. The analytical method is more efficient than the other two methods, so the analytical method proposed in the reference [26] is used to establish the analytical model of velocity effect.

The boundaries of CWE when machining the horizontal plane are shown in Fig. 1(a). Three coordinate systems are established in the figure, which are the tool coordinate system *OXYZ*, the processing coordinate system $O_wX_wY_wZ_w$ and the tool contact coordinate system $PX_cY_cZ_c$, where O is the tool ball center, O_w is the processing zero point, and P is the cutter contact point between tool and machined surface. It should be noted that the CWE model is established in the tool coordinate system *OXYZ*.

The feed direction of the tool is f, and the figure shows the boundaries of the engagement area when the tool feeds along Y_c direction. In this case, the tool engagement area is surrounded by three curves, namely, the

intersection curve AC of the tool hemisphere and the surface to be machined is an arc on the *XOY* plane, the intersection curve BC of the hemisphere and the current cutting layer is an arc in the *XOZ* plane perpendicular to the feed direction, and the intersection curve AB of the hemisphere and the previous cutting layer. It should be noted that BC is the direct contact with the machined surface, and hence the cutter contact point P is located on the curve.

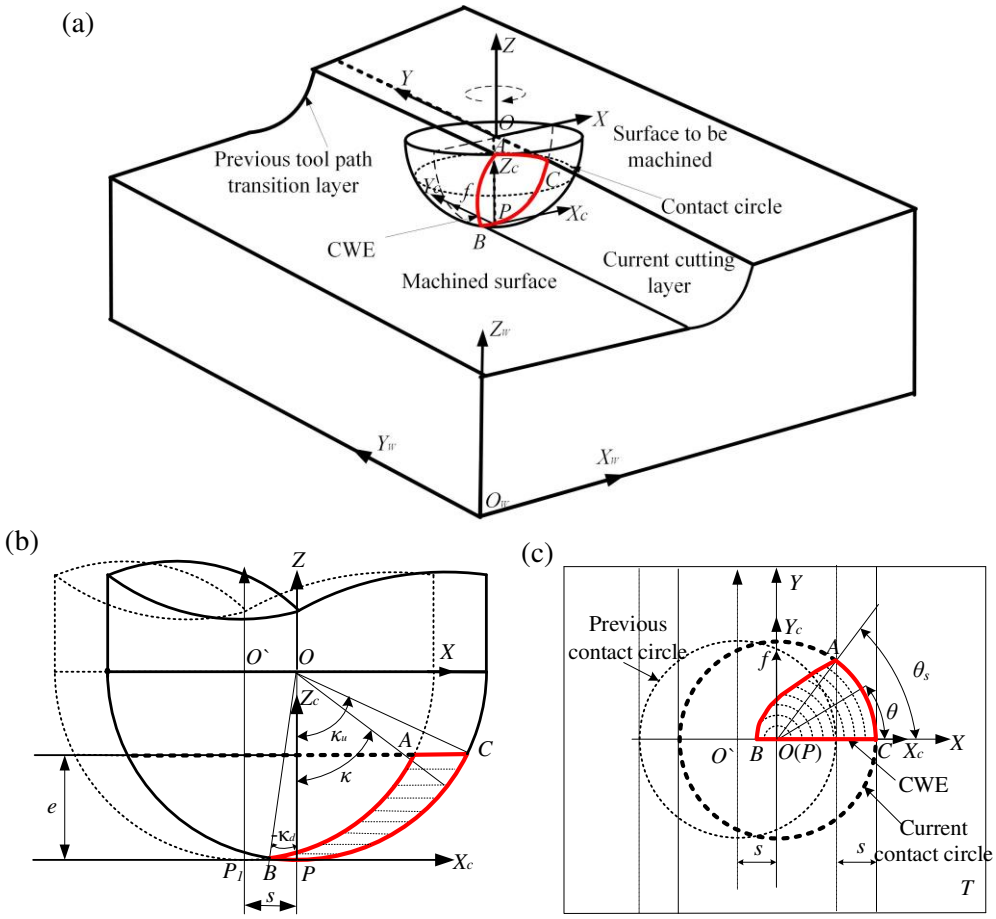

Fig. 1. CWE boundaries of horizontal 3-axis milling with ball-end cutter [26]; (a) 3D view of CWE, (b) left view of CWE and (c) top view of CWE

The analytical model of curve AB is as follows:

$$\begin{cases} x_1 = N.\left(R.\sin\kappa - s\right) \\ y_1 = \sqrt{\left(R\sin\kappa\right)^2 - \left(R\sin\kappa - s\right)^2} \\ z_1 = -R\cos\kappa \\ -\kappa_d \le \kappa \le \kappa_u, \kappa_d = \arcsin(\dfrac{s}{2R}), \kappa_u = \arccos(\dfrac{R-e}{R}) \end{cases} \quad (1)$$

Where, N is the down and up milling coefficient, 1 and -1 for down and up milling, respectively, s is the toolpath stepover; R is tool radius; e is cutting depth; and κ is the axial position angle of the reference point on the cutting boundary. κ is the variable parameter of the analytical expressions. κ_u and $-\kappa_d$ are the upper and lower limits of κ.

The curve BC also takes the axial position angle κ as a variable, and its analytical model can be expressed as follows:

$$\begin{cases} x_2 = N.R.\sin\kappa \\ y_2 = 0 \\ z_2 = -R.\cos\kappa \end{cases} \quad (2)$$

The analytical model of curve AC is as follows:

$$\begin{cases} x_3 = N.\sqrt{R^2-(R-e)^2}.\cos\theta \\ y_3 = \sqrt{R^2-(R-e)^2}.\sin\theta \\ z_3 = e-R \end{cases} \tag{3}$$

Where, θ is the radial position angle of the reference point on the boundary. The value range of θ is: $180°\text{-}\theta_s \le \theta \le 180°$ for down milling, and $0 \le \theta \le \theta_s$ for up milling. θ_s is the phase difference between the two intersections of the contact circle and the CWE boundaries. θ_s can be obtained by the following equation:

$$\theta_s = \arccos\left(\frac{\sqrt{R^2-(R-e)^2}-s}{\sqrt{R^2-(R-e)^2}}\right) \tag{4}$$

According to the geometric relationship between adjacent tool paths shown in Fig. 1(b) and (c), it is easy to obtain the coordinates of A, B and C are as follows:

$$\begin{cases} x_A = N.\left(\sqrt{R^2-(R-e)^2}-s\right) \\ y_A = \sqrt{2s\sqrt{R^2-(R-e)^2}-s^2} \\ z_A = e-R \end{cases}, \begin{cases} x_B = N.\left(-\frac{s}{2}\right) \\ y_B = 0 \\ z_B = -\sqrt{R^2-\left(\frac{s}{2}\right)^2} \end{cases}, \begin{cases} x_C = N.\sqrt{R^2-(R-e)^2} \\ y_C = 0 \\ z_C = e-R \end{cases} \tag{5}$$

The boundaries of CWE of the inclined surface machined by the 3-axis ball-end milling are shown in Fig. 2. Compared with the horizontal plane machining, the position of the tool coordinate system *OXYZ* in the inclined surface machining is unchanged, but the position of P and $PX_cY_cZ_c$ have changed. Therefore, it is necessary to redefine the direction of $PX_cY_cZ_c$, where Z_c points to the spherical center (O) along the normal direction of the machined surface, *Yc* is the projection of the central axis of the tool in the contact plane *T*, and X_c is parallel to the horizontal tangent *t* of the hemisphere at P.

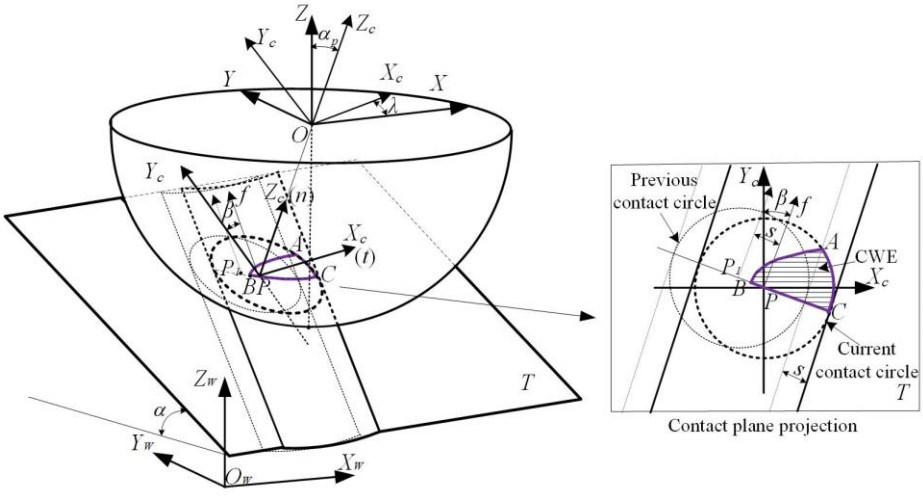

Fig. 2 CWE in three-axis down milling of inclined plane

As shown in Fig. 2, if $PX_cY_cZ_c$ is translated to the spherical center O, the angle between *Z* and Z_c is the machining inclination angle α_p. Both *X* and X_c are on the plane of the hemisphere, and the angle between them is the horizontal rotation angle λ of the oblique plane. The feed direction of the tool is *f*, and the angle between *f* and Y_c is β. The contact plane *T* can be obtained by rotating the horizontal plane around *X* with the angle α_p, and then rotating around Z with the angle λ. Therefore, the CWE model of 3-axis machining oblique plane can be obtained by spatial rotation transformation based on CWE model of 3-axis end milling the horizontal plane. The CWE

model of any feed direction on the inclined surface is expressed as Eq. (6).

$$\begin{cases} \begin{pmatrix} X_i & Y_i & Z_i \end{pmatrix} = \begin{pmatrix} x_i & y_i & z_i \end{pmatrix}.T_Z(\beta).T_X(\alpha).T_Z(\lambda) \\ T_Z(\beta) = \begin{pmatrix} \cos\beta & \sin\beta & 0 \\ -\sin\beta & \cos\beta & 0 \\ 0 & 0 & 1 \end{pmatrix}, T_X(\alpha) = \begin{pmatrix} 1 & 0 & 0 \\ 0 & \cos\alpha_p & \sin\alpha_p \\ 0 & -\sin\alpha_p & \cos\alpha_p \end{pmatrix}, T_Z(\lambda) = \begin{pmatrix} \cos\lambda & \sin\lambda & 0 \\ -\sin\lambda & \cos\lambda & 0 \\ 0 & 0 & 1 \end{pmatrix} \end{cases} \quad (6)$$

where, (x_i y_i z_i) are the coordinates of any point on the boundaries of the engagement area when feeding along Y, (X_i Y_i Z_i) are the rotated coordinates, T_z is the rotation matrix around Z, T_X and is rotation matric around X, β is the feed direction angle, α_p is the machined inclination angle, and λ is the horizontal rotation angle.

2.2 Sensitivity analysis of velocity effect

Usually, the characteristic parameters of the inclined surface in 3-axis machining are the machining inclination angle α_p and the feed direction angle β. The variations of these two parameters will make the CWE area offset longitudinally along the tool hemisphere so that the different positions of the tool participate in the process. However, the change of the horizontal rotation angle λ will only make the engagement area move along the latitude direction on the rotating hemisphere, and this parameter will not change the actual cutting speed. Hence, it does not affect the actual cutting state of ball-end cutters. Therefore, the horizontal rotation angle λ is set to 0° to isolate the influence of α_p and β on the cutting speed distribution in the engagement area.

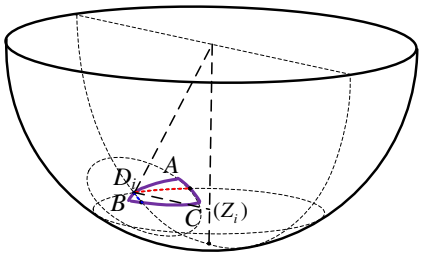

Fig. 3 Geometric relationship of any point on the CWE boundary

The velocity effect studied in this paper refers to the influence of the cutting speed in the material characteristics and chip formation mechanism under a constant feed rate. The point D_i is selected as the reference point on the boundary of the engagement area, as shown in Fig. 3. From the geometric relations, it can be derived the cutting speed V_c at D_i , as shown in Eq. (7), and the feed rate of a ball-end cutter V_f as shown in Eq. (8).

$$V_c = 2\pi.n.R\sin\left[\arccos(\frac{|Z_i|}{R})\right] \quad (7)$$

$$V_f = n.z_n.f_z \quad (8)$$

where n is the spindle speed, z_n is the number of teeth of the cutter, f_z is the feed per tooth, Z_i is the Z coordinate at the reference point.

In a previous work [21], the speed proportional dimensionless number (φ) was proposed, which was defined as the ratio of V_f to V_c. The tool milling performance is described by the value of φ. Without considering the tool wear, the smaller the value of φ is, the better the milling performance is, and its first derivative φ` is used to describe the sensitivity of the tool velocity effect. As $\varphi$` approaches 0, the relative variation of φ decreases, which means that the milling process is more stable. φ and its first derivative φ` are shown in Eq. (9) and (10).

$$\varphi = \frac{V_f}{V_c} = \frac{z_n.f_z}{2\pi.R\sin\left[\arccos(\frac{|Z_i|}{R})\right]} \quad (9)$$

$$\varphi`=\frac{-z_n.f_z.\cos\left[\arccos(\frac{|Z_i|}{R})\right]}{2\pi.R.\sin^2\left[\arccos(\frac{|Z_i|}{R})\right]} \qquad (10)$$

From the construction of the CWE model in the previous section, it can be seen that the CWE boundaries of the ball-end cutter consists of 3 curves. The intersection points A, B, and C of the CWE boundaries are selected as the key points on the engagement area, and the relative changes of CWE are described by the variations of these 3 points. From the CWE model for oblique plane machining, the relationship between the Z coordinates and A, B, C points, α_p and β can be expressed as Eq. (11).

$$\begin{cases} Z_A=\left(\left(\sqrt{R^2-(R-e)^2}-s\right).\sin\beta+\sqrt{2s\sqrt{R^2-(R-e)^2}-s^2}.\cos\beta\right).\sin\alpha_p+\left(e-R\right).\cos\alpha_p \\ Z_B=\sqrt{R^2-(R-e)^2}.\sin\beta.\sin\alpha_p+\left(e-R\right).\cos\alpha_p \\ Z_C=-\dfrac{s.\sin\beta.\sin\alpha_p+\sqrt{4R^2-s^2}\cos\alpha_p}{2} \end{cases} \qquad (11)$$

The CWE models discussed in this paper assume the hypothesis that the contact circle is within the hemisphere of the tool. When the contact circle is just tangent to the hemispheric top circle, as shown in Fig. 4, the maximum inclination angle α_{pmax} is obtained by Eq. (12). In the case of R=5mm, s=0.2mm, e=0.25mm, α_p and β are taken as variables, where the value range of α_p is [0, α_{pmax}], and the value range of β is [-180°, 180°]. The Z coordinate variations of A, B and C are shown in Fig. 5.

$$\alpha_{p\max}=\frac{\pi}{2}-\arccos(\frac{R-e}{R}) \qquad (12)$$

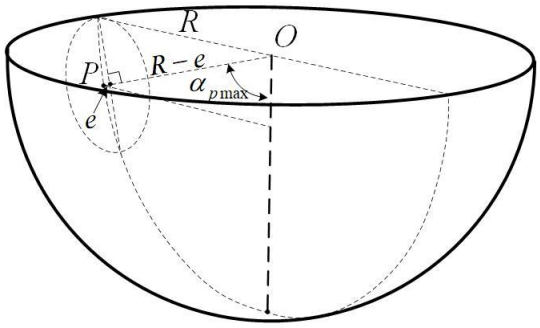

Fig. 4 Contact circle at α_{pmax}

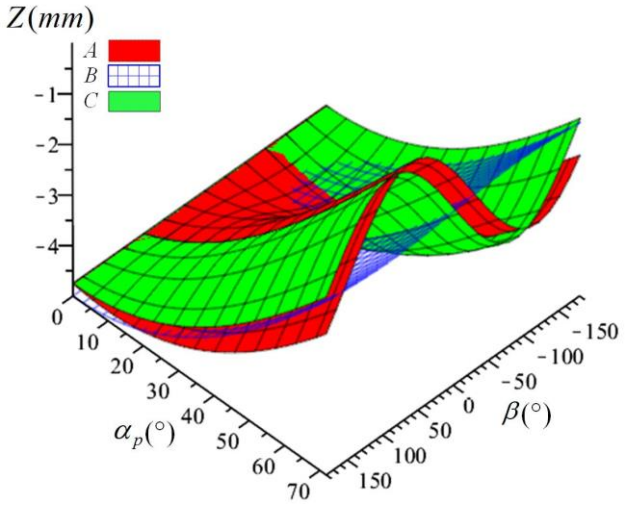

Fig. 5 Variations of Z coordinate.

It can be seen from Fig. 5 that the Z coordinate values of A and C change periodically with the feed direction angle β, and the phase difference is θ_s, which can be obtained by Eq. (4). The Z coordinate value of B is little affected by β.

In the case of the spindle speed n=4000 r/min, by substituting the Z coordinates of points A, B, and C into Eq. (7), the cutting speed surfaces are shown in Fig. 6 (a).

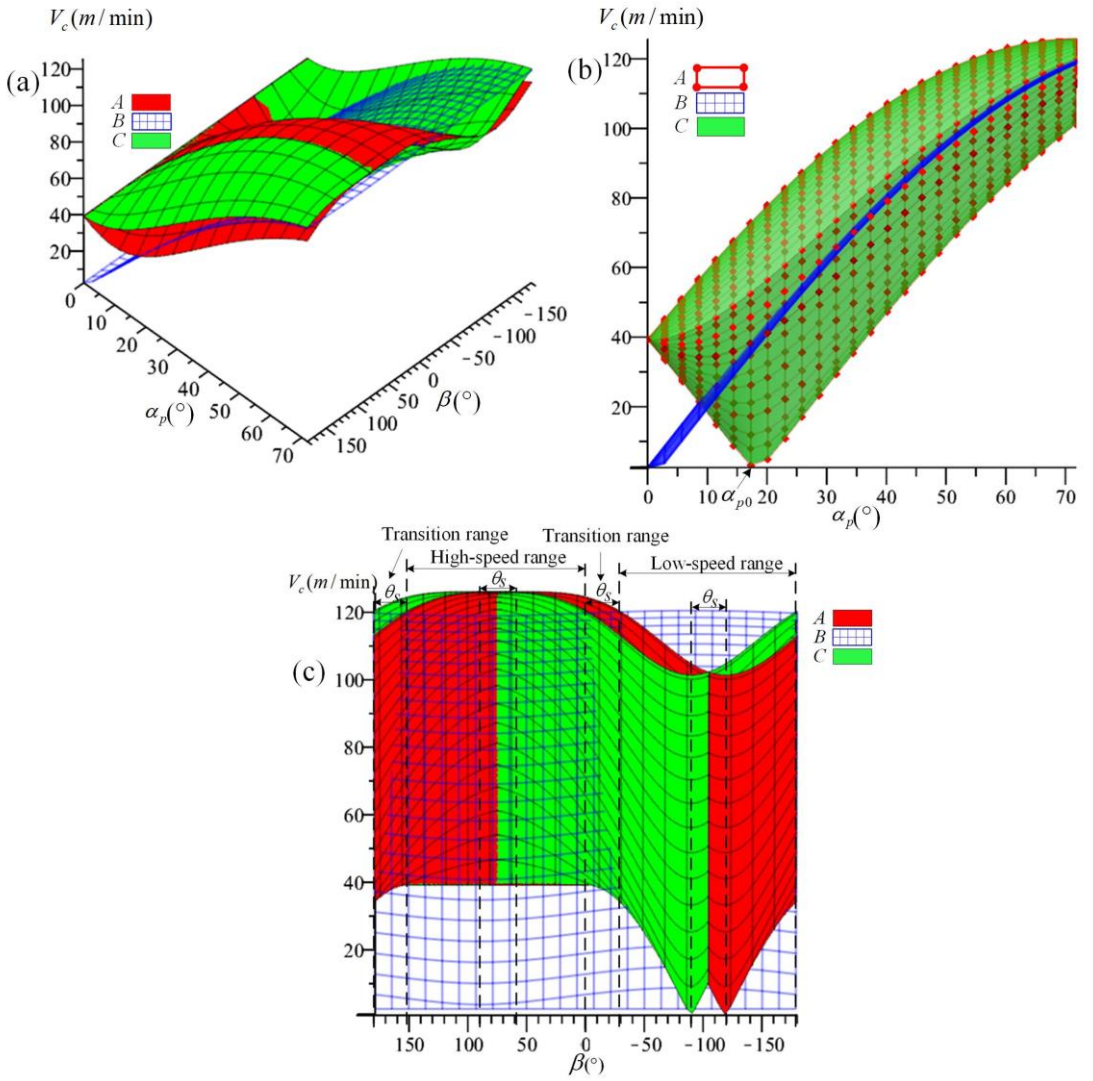

Fig. 6 The cutting speed variations of 3 key points; (a) 3D view of cutting speed surfaces, (b) left view of cutting speed surfaces, (c) front view of cutting speed surfaces

It can be seen from Fig. 6 (a) that the cutting speed values of A and C also vary periodically with β. To further analyze the variations of the cutting speed values of the 3 key points, Fig. 6 (a) is converted into the left view and front view, as shown in Fig. 6 (b) and (c), to facilitate the comparison of the changes of the cutting speed between the two points A and C.

It can be seen from Fig. 6 (b) and (c) that the cutting speed of B is not severely affected by β, but increases with α_p, and the peak and trough values of the surfaces of A and C are the same, which shows that the two points change periodically with the feed direction angle β on the contact circle. When the machining inclination angle conforms to α_p=arccos[(R-e)/R], the contact circle passes through the tool-tip E, as shown in Fig. 7, the trough value of cutting speed at points A and C is 0, and the inclination angle is α_{p0}.

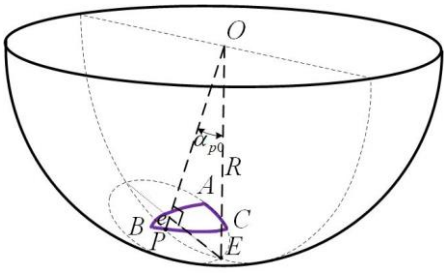

Fig. 7 contact circle passing through tool-tip.

When α_p is in the range of (α_{p0}, α_{pmax}], the tool-tip is on the outside of the contact circle, and the peak and trough of the curved surfaces of point A and C increase with the increase of α_p. When the feed angle β is in the range of [0, 180°-θ_s], the cutting speed values of point A and C are higher than that of point B, the CWE area is located in the upper half of the contact circle, and β is in the high-speed range.

When β is in the range of [-180°, -θ_s], the cutting speed of points A and C are less than that of point B, the CWE area is located in the lower part of the contact circle, and β is in the low-speed range; when β is in the range of [-θ_s, 0] and [180°-θ_s,180°], the cutting speed of point B is between A and C, the engagement area is located in the middle of the contact circle, and β is in transition.

Similarly, for the spindle speed n=4000r/min, tooth number z_n =2, and the feed per tooth f_z=0.15mm, the speed proportion dimensionless number φ and its first derivative φ` are obtained as shown in Fig. 8 (a) and (b).

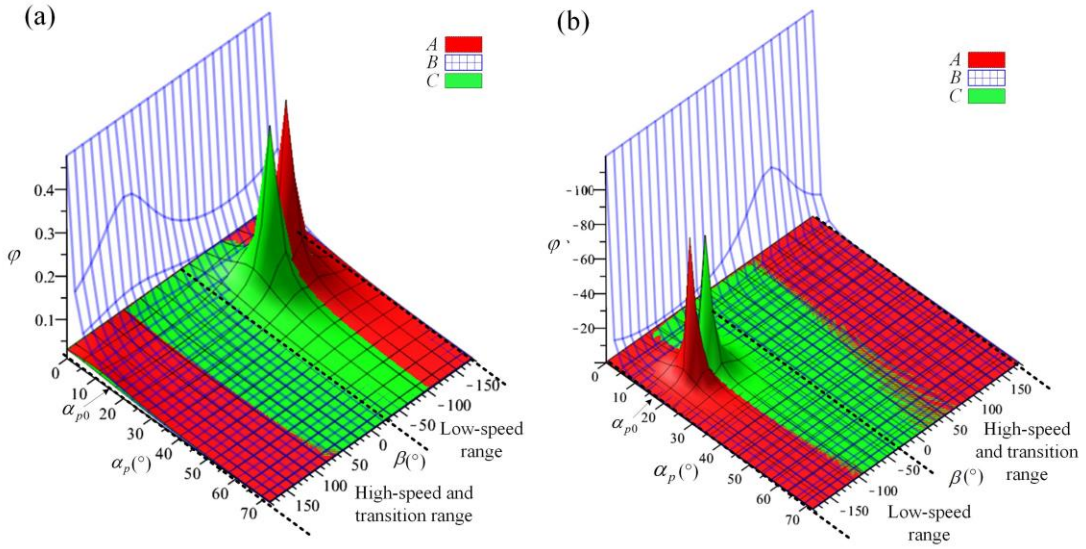

Fig. 8 (a) Speed proportional dimensionless number and (b) first derivative of φ.

As can be seen from Fig. 8 (a) and (b), φ and φ` of B are less affected by the variations of $\beta$, the values of $\varphi$ and $\varphi$` approach 0 for almost all values of β. Only when α_p is close to 0, with the tool-tip participating in the cutting, both φ and φ` deviate from 0, and the milling performance decreases. $\varphi$ and $\varphi$` of A and C are greatly affected by β. When β is in the high-speed range and transition range, it approaches 0 as a whole, and the milling performance of the tool is better. When β is in the low-speed range, φ and φ` of A and C deviate from 0 near α_{p0}, which is when the tool-tip takes part in cutting, and the milling performance of the tool is poor.

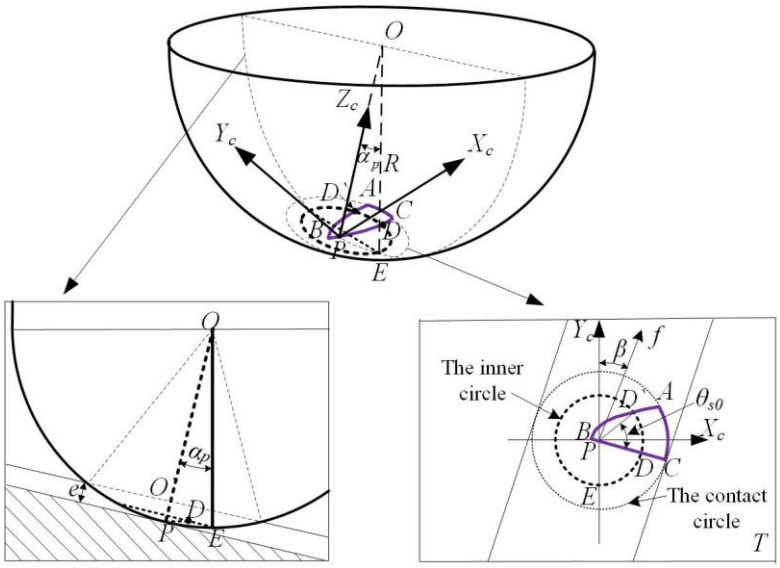

Fig. 9 Geometric relationship of CWE.

When α_p is in the range of [0, α_{p0}], the tool-tip enters the cutting layer and is inside the contact circle. As shown in Fig. 9, with the change of β, the tool-tip may participate in cutting. As the cutting speed near the tool-tip is close to zero, ploughing may occur in the machining process, and the mechanism of material removal will transform from shear to plastic deformation, resulting in poor surface quality, which will also be corroborated in subsequent cutting experiments of this paper. Therefore, to improve the machining surface quality, the tool-tip should be avoided to participate in cutting as far as possible, and the part with a higher cutting speed of the tool should be involved in cutting, so the selection of β is particularly important.

As α_p gradually tends to 0, the trough values of A and C increase, which can no longer represent the minimum cutting speed that may occur in the different feed directions. It can be seen from Fig. 9 that when the tool-tip E enters into the contact circle, the position of the minimum cutting speed has been transferred from the contact circle where A and C are located to the inner circle where the tool-tip E is located. The intersection points of the inner circle and the boundaries CB and AB are recorded as D and D` respectively. The coordinates of D can be obtained by spatial rotation transformation through the point with the axial position angle $\kappa=\alpha_p$ on the boundary of BC in the case of 3-axis end milling horizontal plane, which can be expressed as in Eq. (13).

$$\begin{cases} x_D = N.R.\sin\alpha_p \\ y_D = 0 \\ z_D = -R.\cos\alpha_p \\ \begin{pmatrix} X_D & Y_D & Z_D \end{pmatrix} = \begin{pmatrix} x_D & y_D & z_D \end{pmatrix}.T_z(\beta).T_x(\alpha_p) \end{cases} \tag{13}$$

where, (x_D y_D z_D) are the coordinates of the point with $\kappa=\alpha_p$ on BC in the case of 3-axis end milling horizontal plane, which can be obtained by Eq. (2), and (X_D Y_D Z_D) is the coordinates of D. The phase angle θ_{s0} of D` and D is obtained by Eq. (14), and the coordinates of D` point can be expresses as Eq. (15).

$$\theta_{s0} = N.\arccos(\frac{R.\sin\alpha_P - s}{R.\sin\alpha_P}) \tag{14}$$

$$\begin{pmatrix} X_{D`} & Y_{D`} & Z_{D`} \end{pmatrix} = \begin{pmatrix} x_D & y_D & z_D \end{pmatrix}.T_z(\beta+\theta_{s0}).T_x(\alpha_p) \tag{15}$$

The Z coordinates of D, D`, and P, are shown in Eq. (16), Eq. (17), and Eq. (18), are substituted into Eq. (7). In the case of $n$=4000r/min, the cutting speed surfaces of A, B, C, D, D` and P, can be obtained as shown in Fig.10, where the range of α_p is [0, α_{p0}], and the range of β is [-180°, 180°].

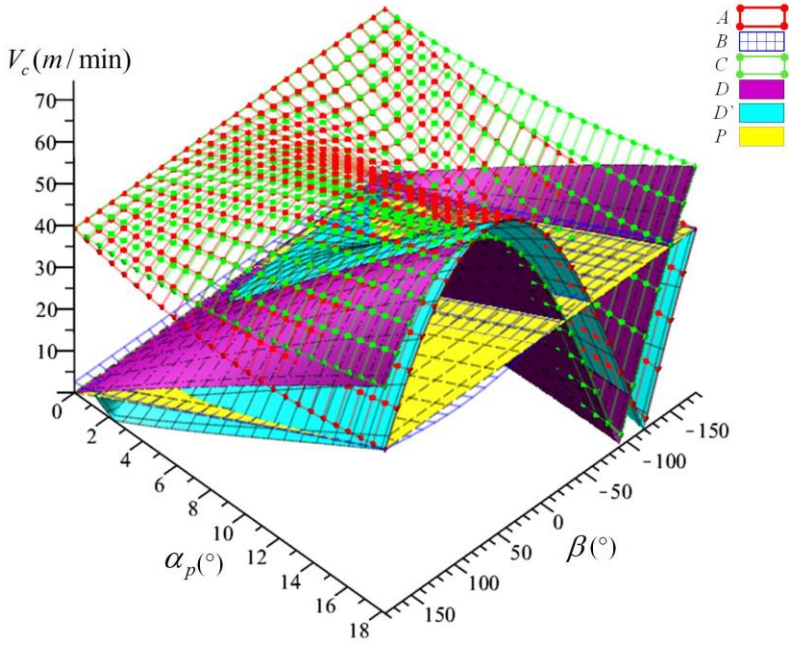

Fig. 10 3D view of cutting speed surfaces

$$Z_D = R.\sin\beta.\sin^2\alpha_p - R.\cos^2\alpha_P \qquad (16)$$

$$Z_{D`} = R.\sin(\beta+\theta_{s0}).\sin^2\alpha_P - R.\cos^2\alpha_P \qquad (17)$$

$$Z_P = -R.\cos\alpha_P \qquad (18)$$

It can be seen from Fig. 10 that the trough values of A and C increase with the decrease of α_p, and the peak values of the wave decrease with the decrease of α_p. Finally, when α_p=0, the cutting speed values of A and C reach the same state in all feed directions. When α_p=α_{p0}, the tool-tip E just passes through the contact circle A and C, and D and D` coincide with C and A, thus the cutting speed values of D and D` in Fig. 10 are coincident with C and A, thus the accuracy of Eq. (16) and Eq. (17) can be verified. When β is in the range of [-90°-θ_{s0}, -90°], the trough values of D and D` are 0, and the tool tip E will enter into the engagement area and participate in the cutting.

3 Optimal conditions of feed direction selection

This section introduces the optimal conditions of the feed direction when the tool tip is inside the contact circle. The CWE area rotates around P with the change of β, that is, P is always in contact with the machined surface and participates in the cutting, the cutting speed of P depends only of α_p, and the distance between B and P is considerably smaller than the length of CWE boundary, hence the cutting speed of B is approximately equal to P. When α_p is in the interval [0, α_{p0}], the cutting speed in the whole engagement area is relatively low. To keep CWE as far away as possible from the tool-tip and avoid the occurrence of the ploughing phenomenon in the cutting process, the tool feed direction β should follow two conditions.

The first condition is that the cutting speed of D and D` is higher than B and P at the same time. In this case, the engagement area can be kept as far away as possible from the tool-tip to ensure that the cutting speed values of the 6 critical points can be at a relatively high-speed range. In order to further investigate the influence of the cutting speed of the 6 points, the surfaces shown in Fig. 10 are converted into a bottom view, shown in Fig. 11. These represent the distribution of the lowest cutting speed points in the engagement area under different machining inclination angles and feed directions.

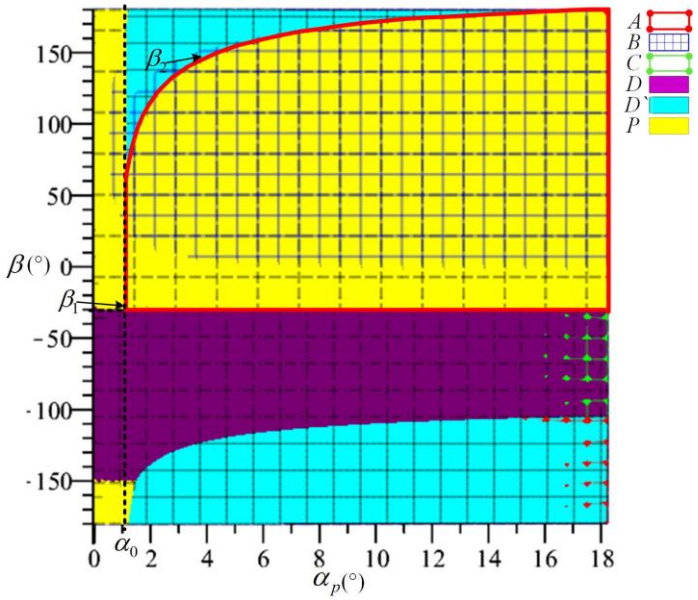

Fig. 11 Bottom view of cutting speed surfaces

When the tool-tip E coincides with the B point, the machining inclination angle is defined as α_0, Eq. (19). When α_p<α_0, the radius of the inner circle is less than the distance of PB, and there is no intersection between the contact inner circle and the boundary curve AB of the engagement area. At this time, α_p is close to 0, and the machining condition is similar to a horizontal plane cutting. In this configuration, the optimization of the feed

direction has little significance.

$$\alpha_0 = \arcsin\left(\frac{s}{2R}\right) \approx 0 \qquad (19)$$

When $\alpha_p > \alpha_0$, the primary selected range of feed direction should satisfy $\beta_1 < \beta < \beta_2$, where β_1 is the intersection line of cutting speed surfaces P and D, which is obtained by Eq. (20) and (21); β_2 is the intersection line of cutting speed surfaces P and D`, and the solving process is modelled as shown in Eq. (22) and (23). The red solid line enclosed area in Fig. 11 is the primary range of the feed direction.

$$Z_D = Z_P \rightarrow R.\sin\beta_1.\sin^2\alpha_p - R.\cos^2\alpha_P = -R.\cos\alpha_P \qquad (20)$$

$$\beta_1 = \arcsin\left(\frac{\cos\alpha_p - 1}{\tan\alpha_p.\sin\alpha_p}\right) \qquad (21)$$

$$Z_{D`} = Z_P \rightarrow R.\sin(\beta_2 + \theta_{s0}).\sin^2\alpha_P - R.\cos^2\alpha_P = -R.\cos\alpha_P \qquad (22)$$

$$\beta_2 = \pi - \beta_1 - \arccos\left(\frac{R.\sin\alpha_P - s}{R.\sin\alpha_P}\right) \qquad (23)$$

However, when β is in the range of [β_1, 0°], as shown in Fig. 12, the minimum cutting speed point in the engagement area is on the boundary BC, which is in direct contact with the machined surface. The cutting state of the cutting edge passing through BC will directly affect the machined surface quality [27]. When the cutting edge participates in cutting from B, the lowest cutting speed on the cutting edge will decrease at first and then rise. The cutting state of the tool will be unstable due to the change of the minimum cutting speed, especially P is closest to the machined surface, which is not conducive to the improvement of the machined surface quality. For a machining inclination angle of α_p=15°, for example, the variation of the cutting speed on BC in different feed directions is shown in Fig. 13. When β=0, P is the position of the lowest cutting speed point on BC, and with the continuous decrease of the feed angle β, the decreasing trend of the lowest cutting speed point in the engagement area is more obvious.

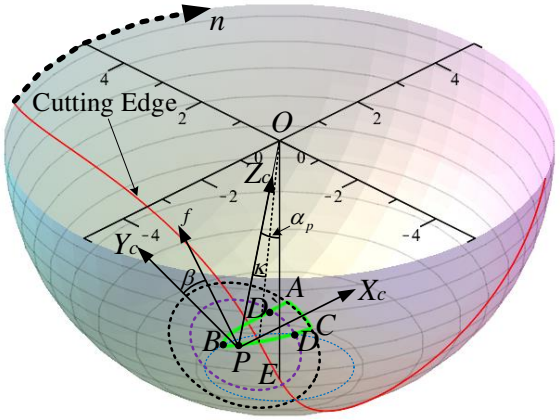

Fig. 12 Geometric analysis of cutting into from B

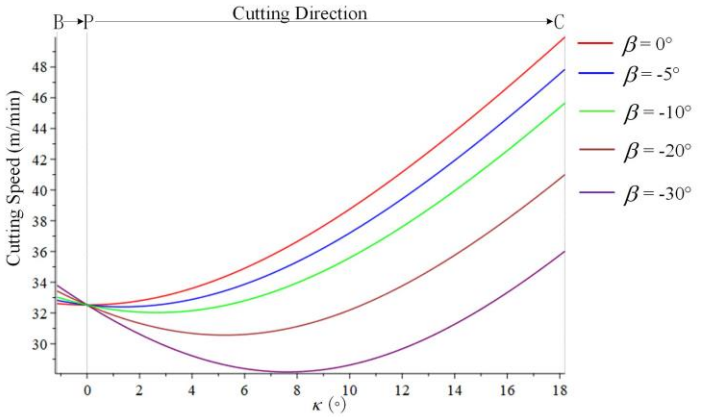

Fig. 13 Variation of cutting speed on boundary BC

Therefore, **the second condition** is that the minimum cutting speed point on the boundary BC is either B or P for the case that the tool participates in cutting from B. To conform to this condition, the Z coordinate value of any point on PC should increase monotonously after the cutting edge passes through P. which is expresses as follows:

$$\begin{cases} Z_{PC} = R.\sin\kappa.\sin\beta.\sin\alpha_p - R.\cos\kappa.\cos\alpha_p \\ 0 \le \kappa \le \kappa_u, \kappa_u = \arccos(\dfrac{R-e}{R}) \end{cases} \qquad (24)$$

Where, Z_{PC} is the Z coordinate value of any point on PC. When the cutting edge passes through any point on BC, there is an axial position angle κ corresponding to it. When κ=0, the intersection position is just at P. By deriving Eq. (24) and making its first derivative Z_{PC}`$\geqslant$0, Eq. (25) can be obtained as follows:

$$Z_{PC}` = \frac{dZ_{PC}}{d\kappa} = R.\cos\kappa.\sin\beta.\sin\alpha_p + R.\sin\kappa.\cos\alpha_p \geq 0 \qquad (25)$$

The solution of Eq. (25) is as follows:

$$\beta \geq -\arcsin\left(\frac{\sin\kappa.\cos\alpha_p}{\cos\kappa.\sin\alpha_p}\right) = -\arcsin\left(\frac{\tan\kappa}{\tan\alpha_p}\right) \qquad (26)$$

where, the machining inclination angle α_p>0, in the right hand side of the equation is monotonically decreasing, and the maximum value of 0 is obtained when κ=0. Under the second condition, the feed direction should conform to $\beta\geqslant$0.

To sum up, when the tool-tip enters the inside of the contact circle, combined with the above two constraints, the feed direction β should be controlled within the optimal range [0, β_2], to keep the engagement area away from the tool-tip and ensure the good cutting condition of the tool.

4 Experimental verification and result analysis

4.1 Cutting experiment

The cutting experiment was set to 15° inclined surface machining, the tool selected was a solid carbide ball end mill with 10mm of diameter (B10), the number of teeth z_n =2, the spindle speed n=4000r/min, the feed rate is 640 m/min, the feed per tooth f_z=0.08mm, the cutting depth e=0.3mm, the toolpath stepover s=0.15mm, and the feed directions β were selected averagely with 16 angles in the range of(-180°,180°]. Under this condition, the CWE area is in the velocity effect sensitive area of the tool, and the tool-tip enters into the contact circle. According to the conditions of feed direction selection before, if the cutting speed in the engagement area is kept in a relatively high-speed cutting state, the feed direction should conform to 0≤β<β_2, where β_2 =181.56°.

The cutting test was carried out on a 3-axis CNC machine tool. The workpiece material was Ti-6Al-4V, and the blank size was 100mm*100mm*50mm. The tilting fixture was used to install the workpiece, and the inclination angle of the fixture was adjusted to 15°. To avoid the error caused by the installation angle of the workpiece, the parallel finishing strategy was used to process the 15° inclined plane before the experiment.

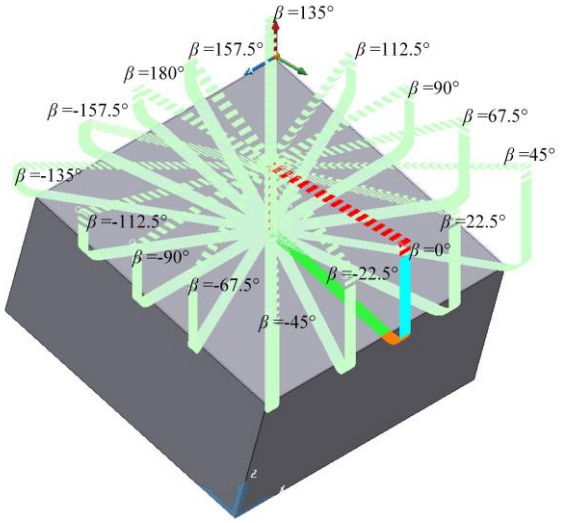

Fig. 14 Tool path for experimental machining.

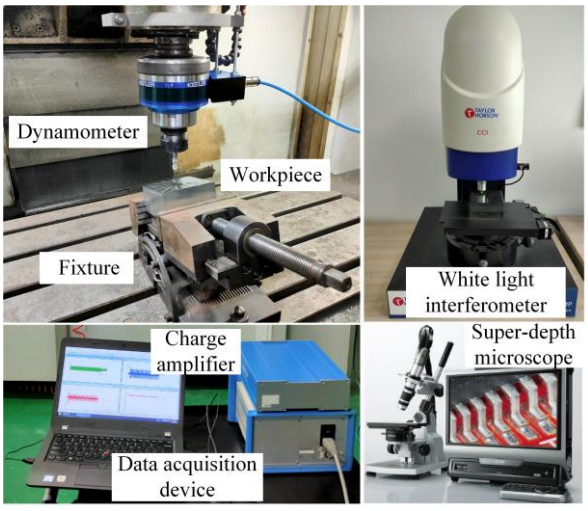

Fig. 15 Instruments and equipment used.

At the beginning of the experiment, a tool (B10) was used for pre-slotting, the tool path for pre-slotting was the first path in the respective feed direction, and then a new tool was replaced to finish the process. The finishing tool paths for experiment are shown Fig. 14, they are all down milling and the cutting was from the outside of the workpiece to the center without coolant. During the cutting process, the KISTLER 9170A rotary dynamometer was

used to measure the milling force, and the chip samples were collected at the end of each cutting. The instruments and equipment used in the machining are shown in Fig. 15.

4.2 Analysis of experimental results

The workpiece after pre-slotting is shown in Fig. 16, it can be seen that there are differences in the machining surface quality in each feed direction, where the groove surfaces quality of the seven paths from -22.5° to -157.5° on the left-hand side are worse than those of other paths. Especially on the paths of -45° and -67.5°, there is an obvious phenomenon of material being torn and peeled off on the side of the cutting-into, however, the side of cutting out is good and neat. (The concept of "cutting into/out" in this paper means that the cutting edge enters into/leaves from the engagement area.) The difference shows that the ball-end cutter is difficult to cut into the workpiece, but the cutting out is relatively stable, which indicates that the material removal mechanism is a combination of plastic deformation (ploughing) and shearing.

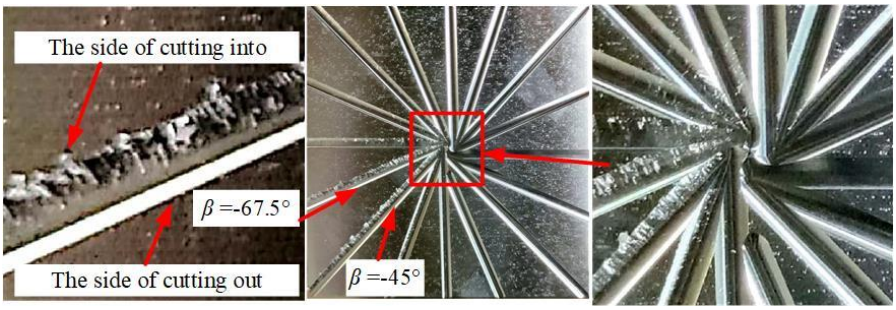

Fig. 16 Workpiece after pre-slotting

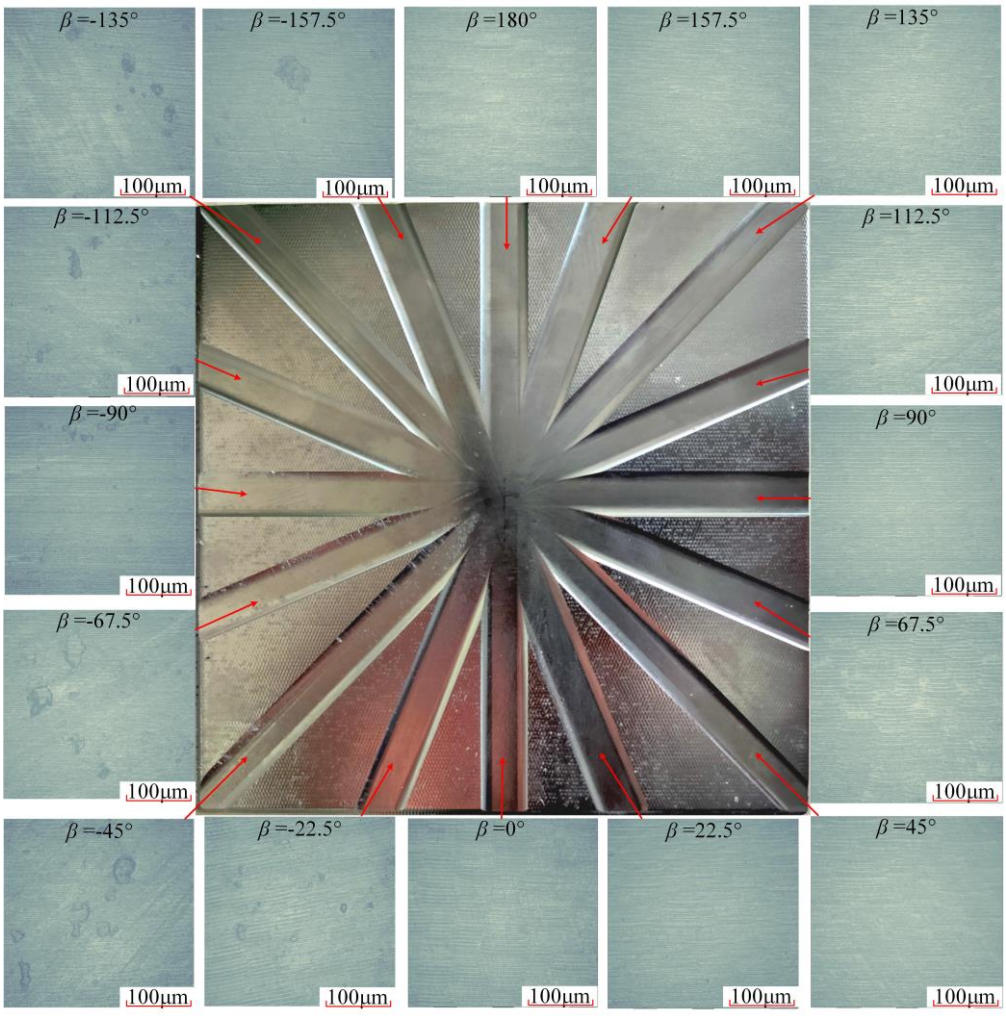

Fig. 17 Surface textures in different directions.

After the finishing process of the experimental workpiece, the white light interference surface profiler (Talysurf CCI) and super-depth microscope (VHX-1000) were used to detect the surface quality of each path, and the machining textures obtained in different directions are shown in Fig. 17. Through the comparison of the machining surface textures in different directions, it can be seen that the machining surfaces on the 9 directions within [0°, 180°] are relatively smooth, with only the normal cutting texture of the tool and no other obvious surface damage. On the 7 directions from -22.5° to -157.5°, beyond the normal cutting texture, there are obvious surface residues on the machined surface, which may be caused by the plastic deformation (ploughing) under poor cutting conditions when the tool is in a low-speed cutting zone.

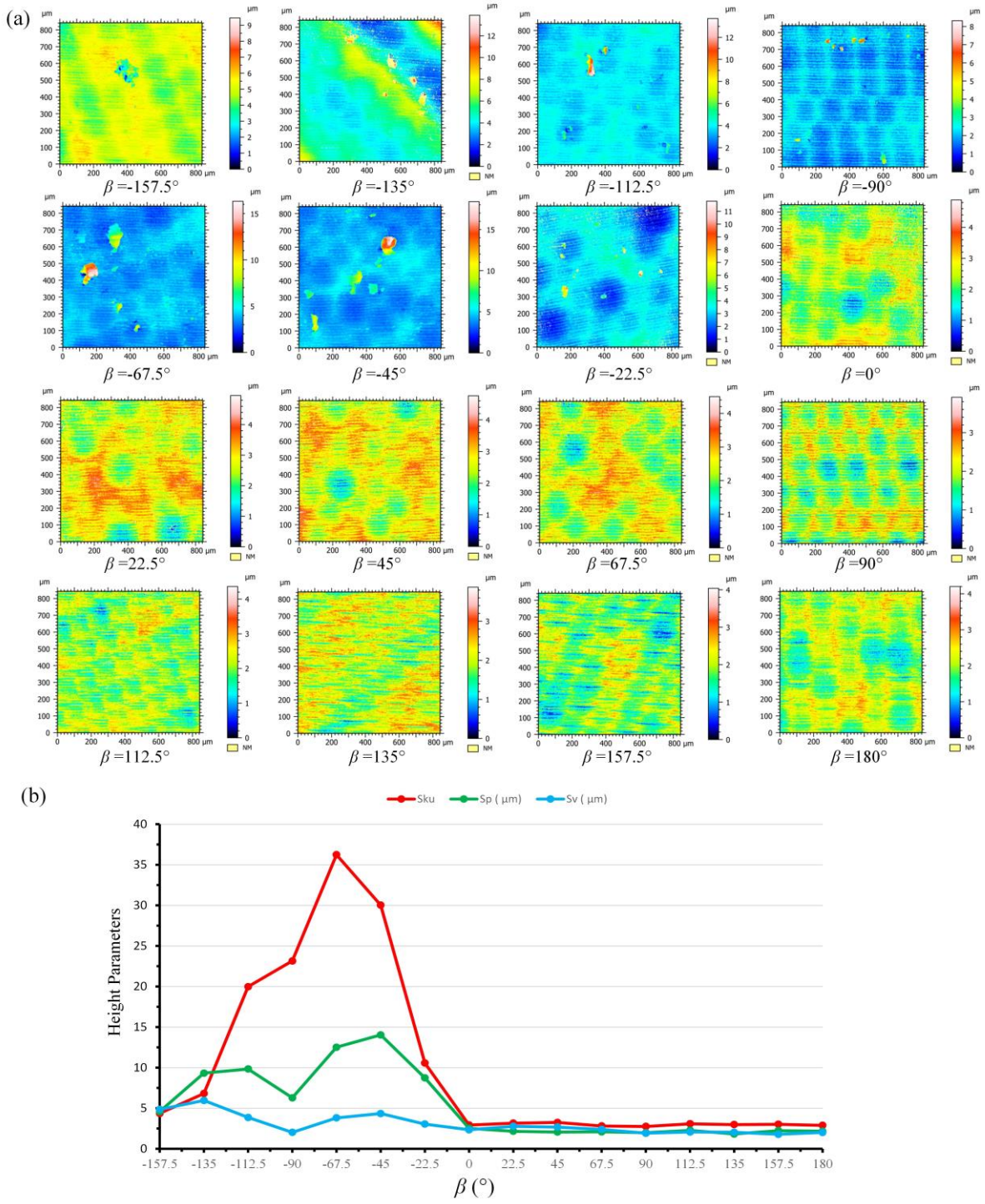

Fig. 18. (a) Surface topographies in different feed directions and (b) Height parameters of surface topographies

The surface topographies of different feed directions are shown in Fig. 18 (a). From the surface topography parameters, it can be seen that the height of machined surface in the feed direction within the range of [0°, 180°] is

0~4 μm, while the residual damage surface corresponding to the feed direction in [-157.5°, -22.5°] is higher than the machined surface, and the height of the surface residue reaches 8~19 μm, which will seriously affect the surface machining quality.

Fig. 18 (b) depicts the changing trend of the height parameters of surface topography in different feed directions. According to the international standard ISO25178, there are three parameters used: *Sku*, *Sp*, and *Sv*. The *Sku* indicates the presence or lack of inordinately high peaks/ deep valleys (*Sku*>3.00) or (*Sku*<3.00), respectively. *Sp* (largest peak height) and *Sv* (largest pit height) are parameters evaluated from the absolute highest and lowest points found on the surface.

From the variation trend of the height parameters in Fig. 18 (b), it can be seen that in the feed direction interval [0°, 180°], *Sku*≈3 indicates that the surface is smooth, and there is no presence of inordinately high peaks or deep valleys caused by surface residual damage. The two values of *Sp* and *Sv* are highly similar and do not produce excessive height differences. However, the *Sku*>3 in the range of [-157.5°, -22.5°], and the difference between *Sp* and *Sv* increases, especially at -45°, -67.5°, -90° and-112.5°, the value of *Sku* reaches more than 20, and gradually improves on -135° and -157.5°, which is due to the position changing of cutting-into and cutting-out on the two paths.

Fig. 19 shows the cutting-into and cutting-out analysis of six directions in the interval [-157.5°, -45°]. Through the geometric relationship of CWE in the figure, it can be seen that the tool cuts into CWE from B in the directions of -45° and -67.5°, as B is very close to the contact point, which is very disadvantageous to cut into from B in the low-speed range. Therefore the surface quality on these two paths are the worst. On the other hand, for the directions of -90° and -112.5°, the position of cutting-into gradually changes from B to C, and the position of cutting out changes from A to B, where the tool-tip of the cutter has completely entered into the CWE, however, the surface quality of these two directions is not the worst. While for the directions of -135° and -157.5°, the cutters are cutting into from A and cutting out from B, although the feed direction is still in the low-speed range, the machined surface quality is improved.

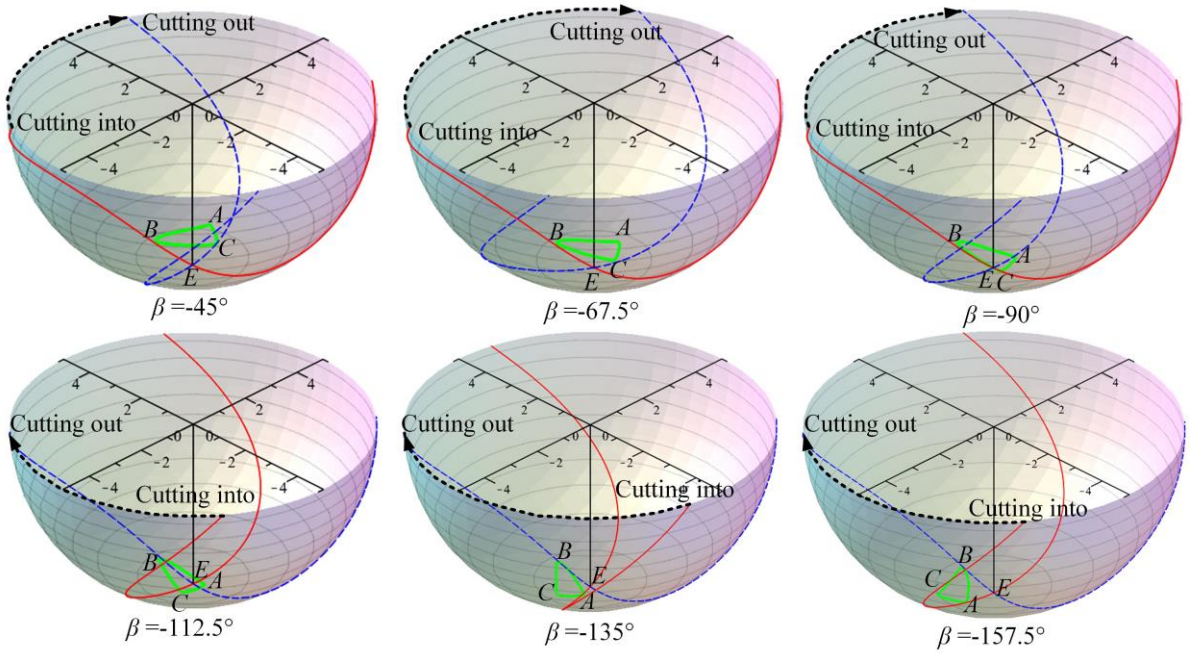

Fig. 19 Analysis of cutting into and out in different feed directions

Fig. 20 illustrates the changes of milling forces in the four feed directions of -45°, 45°, -67.5° and 67.5°, and the force data within 0.048s in the cutting process is obtained, which includes F_a (axial force), F_t (tangential force) and F_r (radial force). This period includes 6-7 cutting-into and cutting-out processes of the tool. Through comparison, it can be seen that the trends of F_a and F_r waveforms are similar for the 45°and 67.5° directions, and

the fluctuation of force during 6-7 cycles of cutting-into and cutting-out can be clearly seen. On the other hand, for the two paths of -45° and -67.5°, it is difficult to find the regular fluctuations of the force caused by cutting-into and cutting-out of the tool, which indicates that the radial tool run-out phenomenon occurred and this process was unstable.

Fig. 20 Comparison of milling force in four feed directions

Fig. 21 shows the tool wear after finishing, Fig. 21 (a) is the rake face and Fig. 21 (b) is the flank face. From the two figures, it can be seen that there is no obvious tool wear or breakage after finishing, which is because the machining parameters selected in this experiment are relatively conservative and the amount of material removal was small. Therefore, the influence of tool wear or breakage on the machined surface quality and milling force can be eliminated.

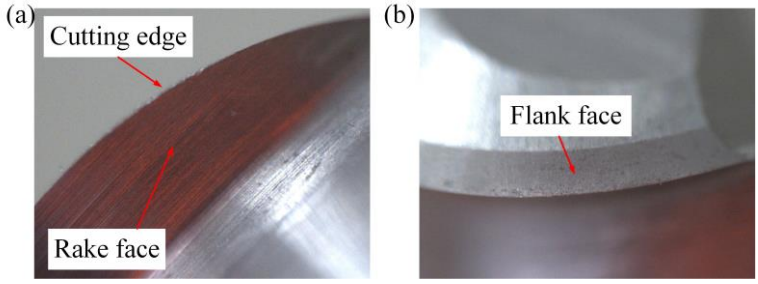

Fig. 21 Tool wear after finishing, (a) rake face, and (b) flank face.

The change of chip shape in different feed directions indicates the variation of cutting mechanism in the process, which has a corresponding impact on the milling process and machined surface quality. Fig. 22 shows the chips in the finishing process in different feed directions, and all the chips in the different directions can be roughly divided into three types.

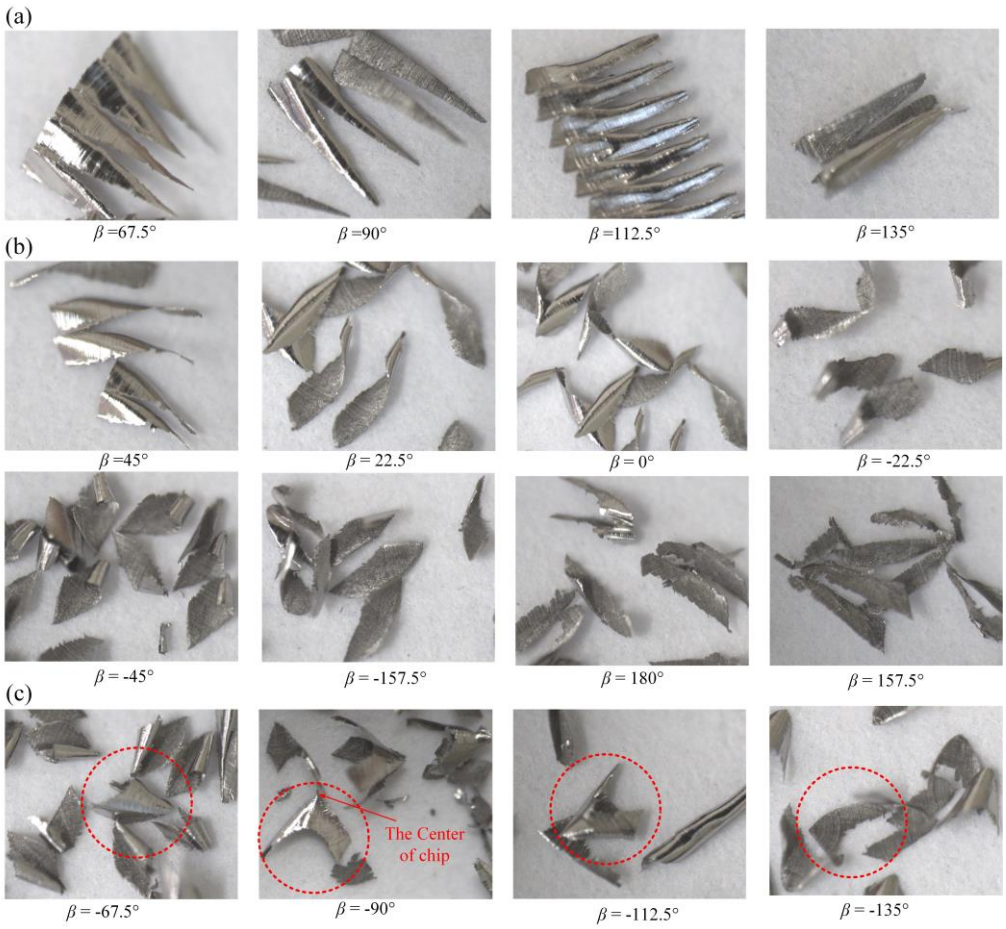

Fig. 22 Comparison of the chip shapes in different feed directions, (a) chips of CWE shape, (b) chips of transition shape and (c) chips of swallow-tailed shape.

The first type is the chips in the feed direction in the range of [67.5°, 135°] as shown in Fig. 22 (a), the shape of the chips in this area is similar to that of CWE, and the edge of the chip is neat, indicating that shearing was the removal mechanism. It should be noted that due to the dry cutting used in this experiment, the higher cutting speed in this range resulted in the increase of cutting temperature and the adhesion between chips, but this does not affect

the quality of the machined surface.

In the second type, as shown in Fig. 22 (b), the chips have twisted gradually in the feed directions of 45°, 22.5° and 0°, but the edges of the chips are still relatively neat. On the other hand, the edges of the chips in the directions of -22.5°, -45°, -157.5°, 180° and 157.5° are no longer neat, indicating that the material removal mode has changed from shearing to plastic deformation and tearing. The chips on the above eight paths are called transitional chips.

The third type of chip is in the feed directions in the range of [-67.5°,-135°] shown in Fig. 22 (c). The shape of this type of chip is similar to the dovetail shape, which is caused by the participation of the tool-tip. In the cutting process, the center of the chip is close to the tool-tip, which will lead to a more serious ploughing phenomenon in these directions.

From the comparisons of surface topographies, milling force states and the shape of chips on different paths, it is shown that within the optimal range [0, β_2] obtained in Section 3, the surface damage caused by ploughing is avoided, and the machined surface quality is improved; while in the non-optimal range, material tearing and plastic deformation caused by ploughing occurs with the deterioration of the machined surface quality, which verifies the effectiveness of the velocity effect sensitive analysis method.

5 Conclusions

In this paper, the chain reactions caused by the velocity effect of ball-end cutters are studied and combined with the cutting-into-out analysis and experimental research, the following conclusions are obtained:

(1) A method for analyzing the velocity effect of the ball-end cutter is established. The result shows that the variation of cutting speed caused by the change of feed direction will have a strong impact on the cutting process when the tool-tip engages in the contact circle.

(2) Several critical positions in the engagement area are selected to describe the variations of cutting speed. Based on the constraint condition that the cutter contact point is located near the lowest cutting speed position, the optimization interval of relatively high-speed feed direction is obtained.

(3) When the feed direction is in the optimized range, the surface quality is better with the tool-workpiece interaction of shearing. However, in the non-optimal interval, the material will have strong plastic deformation and tearing in the process of cutting-into, and the cutting-out process is not affected.

(4) In the feed direction of the non-optimal range, if the tool cuts into the workpiece from the cutter contact point, the surface damage will be aggravated, and correspondingly, cutting out from the tool contact point will improve the machining surface quality.

(5) When the tool-tip engages in the contact circle, with the feed direction changing from positive to negative, the chips will vary from CWE shape to swallow-tailed shape.

References

1. Geng L, Liu P L, Liu K (2015) Optimization of cutter posture based on cutting force prediction for five-axis machining with ball-end cutters. Int. J. Adv. Manuf. Technol 78(5-8):1289-1303 https://doi.org/10.1007/s00170-014-6719-1
2. De Souza A.F, Berkenbrock E, Diniz A.E, Rodrigues, A.R.(2015) Influences of the tool path strategy on the machining force when milling free form geometries with a ball-end cutting tool. J. Brazilian Soc. Mech. Sci. Eng 37(2):675-687 https://doi.org/10.1007/s40430-014-0200-9
3. De Souza A.F, Diniz A.E, Rodrigues A.R, Coelho R T (2014). Investigating the cutting phenomena in free-form milling using a ball-end cutting tool for die and mold manufacturing. Int. J. Adv. Manuf. Technol 71(9-12):1565-1577 https://doi.org/10.1007/s00170-013-5579-4
4. Luo M, Luo H, Zhang D, Tang K(2018) Improving tool life in multi-axis milling of Ni-based superalloy with ball-end cutter based on the active cutting edge shift strategy. J. Mater. Process. Technol 252:105-115 https://doi.org/10.1016/j.jmatprotec.2017.09.010

5. Molnar T.G, Berezvai S, Kiss A.K, Bachrathy D., Stepan G (2019) Experimental investigation of dynamic chip formation in orthogonal cutting. Int. J. Mach. Tools Manuf 145: 103429 https://doi.org/10.1016/j.ijmachtools.2019.103429
6. Ning L, Veldhuis S.C, Yamamoto K (2008) Investigation of wear behavior and chip formation for cutting tools with nano-multilayered TiAlCrN/NbN PVD coating. Int. J. Mach. Tools Manuf 48(6):656-665 https://doi.org/10.1016/j.ijmachtools.2007.10.021
7. Rowe W.B, Bell W.F, Brough D, Davies B.J (1986) Optimization Studies in High Removal Rate Centreless Grinding. CIRP Ann. - Manuf. Technol 35: 235–238. https://doi.org/10.1016/S0007-8506(07)61878-2
8. Tian L, Fu Y, Yang L, Xu J, Li H, Ding W (2013) Investigations of the “speed effect” on critical thickness of chip formation and grinding force in high speed and ultra-high speed grinding of superalloy. Jixie Gongcheng Xuebao (in Chinese)/Journal Mech. Eng 49, 169–177. https://doi.org/10.3901/JME.2013.09.169
9. Liu X, Ma J, Yue C, Wan Q (2017) Determining the minimum cutting thickness (MCT) of hardened steel based on ball end milling method. Jixie Gongcheng Xuebao (in Chinese)/Journal Mech. Eng 53(1): 180-189 https://doi.org/10.3901/JME.2017.01.180
10. Lee C.M, Kim S.W, Lee Y.H, Lee D.W (2004) The optimal cutter orientation in ball end milling of cantilever-shaped thin plate. J. Mater. Process. Technol 153-154(22):900-906 https://doi.org/10.1016/j.jmatprotec.2004.04.106
11. Daymi A, Boujelbene M, Linares J. M, Bayraktar E, Ben Amara A. (2009) Influence of workpiece inclination angle on the surface roughness in ball end milling of the titanium alloy Ti-6Al-4V. Journal of Achievements in Materials and Manufacturing Engineering 2009, 35(1):79-86 https://doi.org/10.2307/20788690
12. Kalvoda T, Hwang Y.R (2009) Impact of various ball cutter tool positions on the surface integrity of low carbon steel. J. Mater. Des 30(9):3360-3366 https://doi.org/10.1016/j.matdes.2009.03.039
13. Yao C.F, Wu D.X, Jin Q.C, Huang X.C, Ren J.X, Zhang D.H (2013) Influence of high-speed milling parameter on 3D surface topography and fatigue behavior of TB6 titanium alloy. J. Trans. Nonferrous Met. Soc. China (English Ed) 23(3): 650- 660 https://doi.org/10.1016/S1003-6326(13)62512-1
14. Shen X., Zhang D, Tan L (2020) Effects of cutter path orientations on milling force, temperature, and surface integrity when ball end milling of TC17 alloy. J. Proc. Inst. Mech. Eng. Part B J. Eng. Manuf 2020(7):1-13 https://doi.org/10.1177/0954405420971070
15. Nicola G.L, Missell F.P, Zeilmann R.P (2010) Surface quality in milling of hardened H13 steel. Int. J. Adv. Manuf. Technol 49(1-4):53-62 https://doi.org/10.1007/s00170-009-2382-3
16. Aspinwall D.K, Dewes R.C, Ng E.G, Sage C, Soo S.L (2007) The influence of cutter orientation and workpiece angle on machinability when high-speed milling Inconel 718 under finishing conditions. Int. J. Mach. Tools Manuf 47(12-13):1839-1846 https://doi.org/10.1016/j.ijmachtools.2007.04.007
17. Tan L, Yao C, Ren J, Zhang D (2017) Effect of cutter path orientations on cutting forces, tool wear, and surface integrity when ball end milling TC17. Int. J. Adv. Manuf. Technol 88(9-12):2589-2602 https://doi.org/10.1007/s00170-016-8948-y
18. Toh C.K (2005) Comparison of chip surface temperature between up and down milling orientations in high speed rough milling of hardened steel. J. Mater. Process. Technol 167(1):110-118 https://doi.org/10.1016/j.jmatprotec.2004.10.004
19. Toh C.K (2004) Surface topography analysis in high speed finish milling inclined hardened steel. J. Precis. Eng 28(4):386-398 https://doi.org/10.1016/j.precisioneng.2004.01.001
20. Chen X X, ZHAO J, ZHANG W W (2019) Optimization analysis considering the cutting effects for high-speed five-axis down milling process by employing ball end mill. Int. J. Adv. Manuf. Technol 105(1):(5-8) https://doi.org/10.1007/s00170-019-04436-0
21. Zhang A. S, Liu X. L, Yue C. X, Yang S. C, Xia W (2020) Analysis of Minimum Cutting Speed in Velocity Effect Sensitive Area of Ball End Mill. Jixie Gongcheng Xuebao (in Chinese) /Journal Mech. Eng 56(11):229

https://doi.org/10.3901/JME.2020.11.229
22. Kim G M, Cho P J, Chu C N (2000) Cutting force prediction of sculptured surface ball-end milling using z-map. Int. J. Mach. Tools Manuf 40(2):277-291 https://doi.org/10.1016/S0890-6955(99)00040-1
23. Lazoglu I. (2003) Sculpture surface machining: a generalized model of ball-end milling force system. Int. J. Mach. Tools Manuf 43(5): 453-462 https://doi.org/10.1016/S0890-6955(02)00302-4
24. Imani B M, Sadeghi M H, Elbestawi M A (1998) An improved process simulation system for ball-end milling of sculptured surfaces. Int. J. Mach. Tools Manuf 38(9):1089-1107 https://doi.org/10.1016/S0890-6955(97)00074-6
25. Wei Z C, Wang M J, Zhu J N (2011) Cutting force prediction in ball end milling of sculptured surface with Z-level contouring tool path. Int. J. Mach. Tools Manuf 51(5):428-432 https://doi.org/10.1016/j.ijmachtools.2011.01.011
26. Wei Z,C Wang M J, Wang X W, Zhao D Y (2017) A semi-analytical cutter workpiece engagement model for ball end milling of sculptured surface. Jixie Gongcheng Xuebao (in Chinese) /Journal Mech. Eng 53(1):198-205 https://doi.org/10.3901/JME.2017.01.198
27. Habibi M, Kilic Z.M, Altintas Y (2021) Minimizing Flute Engagement to Adjust Tool Orientation for Reducing Surface Errors in Five-Axis Ball End Milling Operations. J. Manuf. Sci. Eng 143(2):1-35 https://doi.org/10.1115/1.4048267

Nomenclature

$OXYZ$	tool coordinate system	Z_i	the Z coordinate at any reference point
$O_wX_wY_wZ_w$	processing coordinate system	$[T_z]$, $[T_x]$	rotation matrices around Z and X
$PX_cY_cZ_c$	tool contact coordinate system	V_f	feed rate
f	tool feed direction	V_c	cutting speed
N	down and up milling coefficient	φ, φ `	speed proportional dimensionless number and it's first derivative
s	toolpath stepover		
R	tool radius	n	spindle speed
e	cutting depth	z_n	tooth number
κ	axial position angle	f_z	feed per tooth
θ	radial position angle	CWE	Cutter Workpiece Engagement
θ_s	phase difference	P	Cutter contact point
β	feed direction angle	A, B, C	Intersection points of CWE boundaries
α_p	machined inclination angle	D, D`	Intersection points between CWE boundaries and the inner circle
λ	horizontal rotation angle		
D_i	reference point on CWE		